JOURNAL OF MATERIALS SCIENCE **37** (2002) 5159–5165

The rate dependent response of a titanium alloy subjected to quasi-static loading in ambient environment

W. ZHOU
Division of Engineering & Applied Sciences, Harvard University, 9 Oxford Street, Cambridge, MA 02138, USA
E-mail: wzhou@cantab.net

K. G. CHEW
Singapore Technologies Automotive Ltd., 5 Portsdown Road, Republic of Singapore

A dual phase Ti-6A1-4V alloy was tested in uniaxial tension over a large quasi-static loading range (10^{-5}–10^{-1} s^{-1}) in ambient environment. As strain rate increases, strength of the alloy was found to increase at the expense of ductility. In the low strain-rate region, strain rate sensitivity of the material experienced a gradual decrease during plastic deformation. In the high strain-rate region, strain-rate sensitivity of the material was largely constant for most part of the plastic deformation. The different rate dependent behaviours are believed to be caused by a change of governing plastic deformation mechanism from dislocation slip at low strain rates to twinning at the highest strain rate. Strong fractographic and metallographic evidence was obtained to understand the micromechanisms of plastic deformation.

1. Introduction

Titanium alloys have superior specific strength and excellent corrosion resistance. For many decades, they have been used in aerospace structures [1]. In the recent years, their applications have expanded rapidly. Products of titanium alloys can now be found in automobiles, sports equipment, fashion apparels, land and marine architectures, medical implants, gas turbine engines, and armoured vehicles [2, 3].

Over the years, considerable researches have been carried out to improve the mechanical properties of titanium alloys such as strength, ductility and fatigue resistance [4–7]. Many studies were also conducted to understand the relationship among chemical composition, processing parameters, microstructures and properties of the materials [8, 9] or to understand the fracture behaviour in corrosive environments [10, 11] or at very high strain rates [12, 13]. However, it is surprising that few researches have been devoted to understanding the strain rate sensitivity of titanium alloys subjected to quasi-static loading in the ambient environment.

In the present study, a titanium alloy of the Ti-6A1-4V type was tested in uniaxial tension over a large quasi-static loading range (0.1–1000 mm/min) at room temperature. It is interesting to observe that the material exhibits considerable sensitivity to strain rate within the designated test range. Normally, rate dependent study of materials involves arriving at an accurate constitutive relation for computer simulations [14–16]. For the current investigation, attention was focused mainly on elucidating the *micromechanisms* of deformation underlying the rate dependent response of the titanium alloy in the quasi-static loading range. The effect of deformation *micromechanisms* is important because of their profound influence on material properties [17].

Another significant part of this study was the ability to carry out tensile test at a high loading rate (i.e., 1000 mm/min) and simultaneously acquire useful test data digitally. The tension data obtained at various loading rates were used to plot *true stress* versus *true strain* curves. They were also used to plot curves of *strain rate sensitivity* versus *strain* at representative strain-rate regions in the quasi-static loading range. The curves obtained were studied in accordance with the physical findings.

2. Experimental

The titanium alloy used in the study was hot-rolled into plates of 15.9 mm thickness. After hot rolling, the material was left in the annealed state at 1033 K for 8 hours. The fabrication process produced a microstructure with grains elongated in the rolling direction and flattened in the short-transverse direction. The average grain size was about 10 μm. The chemical composition of the material is given in Table I.

Cylindrical tensile specimens were standard *ASTM E8-98* specimens of 35.6 mm in gauge length and 8.9 mm in diameter. All the specimens were machined in the longitudinal orientation of the hot-rolled plate.

TABLE I Chemical composition of titanium alloy Ti-6A1-4V (in wt%)

C	Fe	N	Al	V	O	Ti
0.012	0.190	0.008	6.380	4.070	0.170	Balance

The tension testing was carried out over a wide quasi-static loading range of 0.1, 10 and 1000 mm/min (i.e., 4.68×10^{-5}, 4.68×10^{-3} and 4.68×10^{-1} s^{-1}) at room temperature using a servo-hydraulic Instron machine of 250 kN capacity. An extensometer with 25 mm gauge length and 5 mm working distance was used to monitor the true displacement (rather than the machine crosshead displacement). The testing data were acquired automatically using a computer system and processed using classical equations to plot *true stress* versus *true strain* curves. The gauge length was marked on the tensile specimens before testing. After testing, the corresponding length at fracture and the neck diameter at fracture were measured for all the specimens. The fracture surfaces of the tensile specimens were carefully examined using the scanning electron microscope (SEM).

Microstructural study was performed using the optical microscope, SEM and transmission electron microscope (TEM). The metallographic and thin foil samples were obtained from the necked region of tested tensile specimens sectioned using a slow speed diamond cutter. The sectioned samples were ground on SiC paper, electropolished and chemically etched for observation. The electropolishing was performed in an electrolyte of 900 ml acetic acid (99.8%) and 100 ml perchloric acid (60%) at 25 volts for about 1 min, and etching was carried out in a solution of 5% HF, 20% HNO_3 and 75% glycerol for approximately 30 s.

3. Experimental results

Microstructure of the titanium alloy was found to consist of α and β phases, as shown in Fig. 1. The bimodal $\alpha + \beta$ microstructure contains bulky primary α grains, and alternate α and β platelets. It can be seen from the figure that the primary α grains are elongated in one direction. This is the result of hot rolling.

TABLE II Comparison of tensile properties at three different strain rates

Strain rate (s^{-1})	0.2% yield stress (MPa)	UTS (MPa)	Elongation (%)	Young's modulus (GPa)
4.68×10^{-5}	871	955	15.7	119
4.68×10^{-3}	951	987	14.3	120
4.68×10^{-1}	1030	1053	13.3	120

A summary of tensile properties obtained at different strain rates (based on the average of two tests) is given in Table II. It can be seen clearly from the table that flow stress of the titanium alloy increases with increasing strain rate. The tensile ductility as measured by elongation is shown in Table II to decrease with increasing strain rate.

Typical *true stress* versus *true strain* curves (also referred to as the flow curves) are shown in Fig. 2. The small slope of the curves in the plastic range indicates that the titanium alloy generally possesses a low strain hardening rate. At the highest strain rate (flow curve C), the flow stress reaches a peak before softening, followed by the final sudden fracture. The decrease in flow stress of a material during plastic deformation has been commonly attributed to the thermal softening effect [18].

4. Discussion

Both Table II and Fig. 2 show the dependence of flow stress (σ) on strain rate ($\dot{\varepsilon}$) in the quasi-static loading range. The strain rate sensitivity curves (i.e., $\log \sigma$ versus $\log \dot{\varepsilon}$) in Fig. 3 illustrate this rate dependence more clearly. The strain rate sensitivity (m) is given by the following equation [19],

$$\sigma = C(\dot{\varepsilon})^m \tag{1}$$

Therefore, it can be seen from Fig. 3 that strain-rate sensitivity of the titanium alloy generally becomes

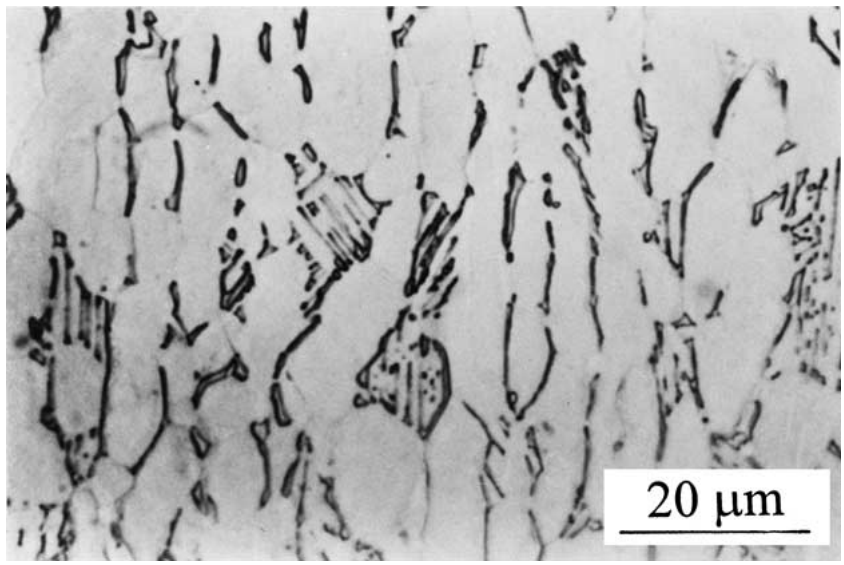

Figure 1 Optical micrograph showing the microstructure of the Ti-6A1-4V type titanium alloy to consist of generally elongated primary α grains and α and β platelets. It is noted that the β platelets appear dark or black under the optical microscope.

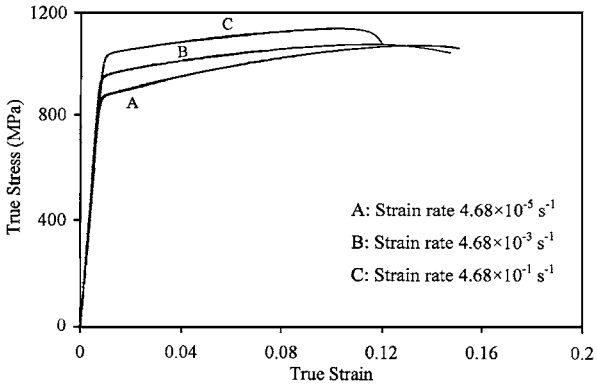

Figure 2 True stress versus true strain curves for the Ti-6A1-4V type titanium alloy tested at three different strain rates.

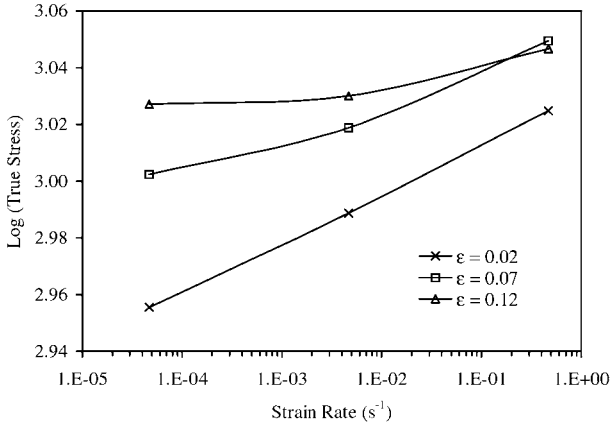

Figure 3 The influence of strain rate on the flow stress of the titanium alloy presented for three levels of plastic strain. The strain rate sensitivity of the material is observed to vary inversely with plastic strain.

smaller at higher plastic strain level. For any given range of strain rate, the strian rate sensitivity can be plotted directly as a function of plastic strain using the formula below [19],

$$m = \left(\frac{\partial \log \sigma}{\partial \log \dot{\varepsilon}}\right) \approx \left(\frac{\Delta \log \sigma}{\Delta \log \dot{\varepsilon}}\right) = \frac{\log \sigma_2 - \log \sigma_1}{\log \dot{\varepsilon}_2 - \log \dot{\varepsilon}_1} = \frac{\log(\sigma_2/\sigma_1)}{\log(\dot{\varepsilon}_2/\dot{\varepsilon}_1)} \quad (2)$$

Fig. 4 shows the relationship between the strain rate sensitivity and plastic strain for four typical strain-rate regions. The strain rate sensitivity of the material is seen to decrease gradually during plastic deformation in the low strain-rate region but remain largely constant before a sharp drop in the high strain-rate region. The variation of m with plastic strain is an indication of the microstructural changes during plastic deformation [20].

Visual observation of the broken halves of the tensile specimens revealed that the overall fracture path was orientated at roughly 45 degrees to the tensile loading axis, as shown in Fig. 5. In a specimen loaded in uniaxial tension, the direction of maximum shear stress is at 45 degrees to the loading axis. Therefore, it is plausible to deduce that fracture of the tensile specimens is by a shear process. Fractographic observation under the SEM provided further evidence to support this argument. As shown in Fig. 6, the fracture surfaces contain highly elongated or drawn out dimples, which are features typical of those obtained in a shear fracture [21].

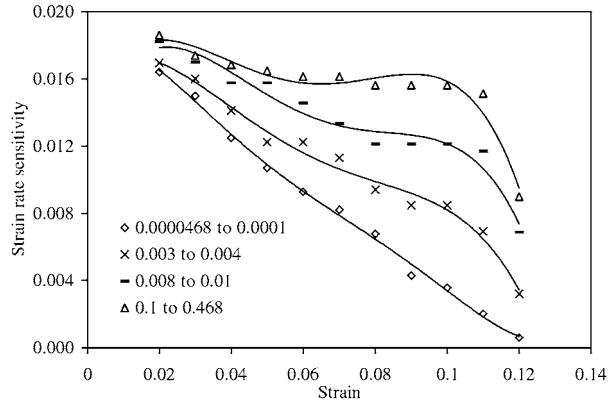

Figure 4 The variation of strain rate sensitivity with plastic strain illustrated for four strain-rate regions.

Fracture surfaces of the specimens tested were carefully observed under the SEM to identify the specific microstructural features associated with the initial stage of plastic deformation. The observation revealed that the fracture was predominantly transgranular. However, no clue was obtained to understand the micromechanical process of deformation and fracture. Therefore, the deformation and fracture process was further studied using specially prepared metallographic samples, which were made by sectioning the broken halves of the tensile specimens along the loading axis. After the samples were electropolished and chemically etched, they were observed under an optical microscope of high resolution or SEM. Figs 7 and 8 show microcracks located in the highly strained region just below the fracture surface.

It is very interesting to note from Figs 7 and 8 that all the microcracks were initiated at grain boundaries. They were located either along primary α grain boundaries or at α/β interfaces. The crack initiation at *grain boundaries* is in sharp contrast to the observation that the final fracture of the tensile specimens was largely of the *transgranular* type (see Fig. 6).

Orientation of the grain-boundary microcracks is noteworthy. As shown clearly in Fig. 7, almost all the microcracks were oriented at roughly 45 degrees to the loading axis, i.e., in the direction of the maximum shear stress (τ_{max}). This observation indicates strongly that the microcracks were formed due to grain-boundary sliding under the action of τ_{max} during tensile loading. Fracture or creep in the form of grain boundary sliding is not an unusual phenomenon for metallic materials tested at elevated temperatures [22–24]. However, it seems to be a rare observation that fracture of Ti-6A1-4V alloy at room temperature is caused by microcracks initiated at grain boundaries. Similar to the void coalescence process in ductile fracture of steels [25], the final fracture of the titanium alloy is probably by coalescence of grain boundary microcracks along the direction of τ_{max}, as shown in Fig. 9.

Furthermore, the governing mechanism of deformation at high strain rate ($4.68 \times 10^{-1}\ s^{-1}$) was found to be twinning, as shown in Fig. 10. The twin features were

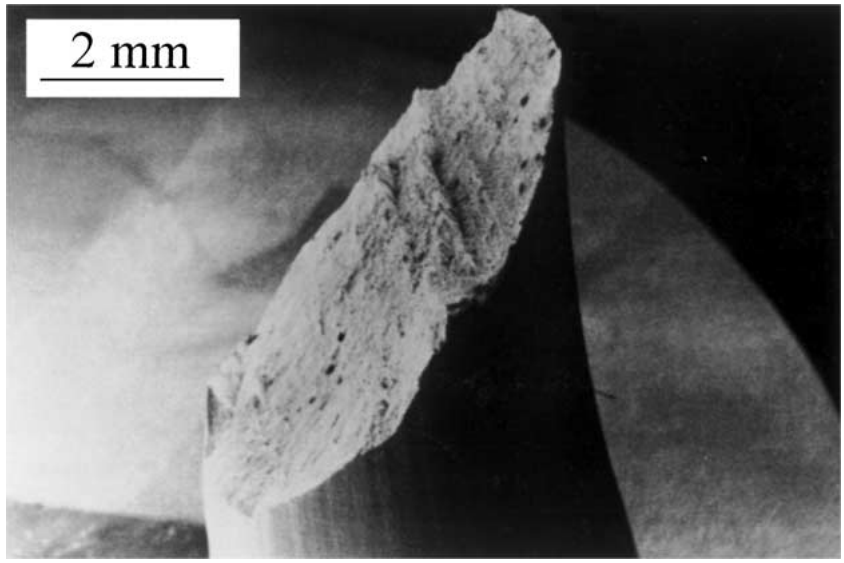

Figure 5 A typical fracture surface observed in the titanium alloy subjected to uniaxial tension at the different strain rates. The fracture surface is observed to be at roughly 45° to the loading axis (vertical) under the SEM.

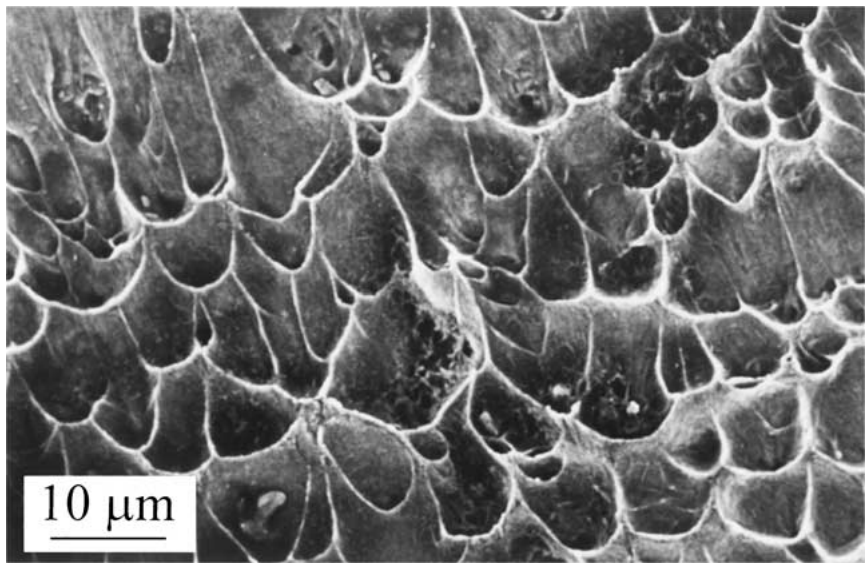

Figure 6 Shear dimples observed in a tested tensile specimen deformed at the highest strain rate of $4.68 \times 10^{-1}\ s^{-1}$.

observed in the necked region of specimens sectioned in the direction normal to the loading axis. Twins were also observed under the TEM and a close up of the deformation feature is given in Fig. 11. It is noted that twinning features were rarely observed in the neck region of specimens tested at the lowest strain rate ($4.68 \times 10^{-1}\ s^{-5}$). The study shows that higher loading rates tend to promote twinning and suppress slip. The observation of twinning in the present study is in contrast to the belief that deformation of materials under quasi-static loading is generally by dislocation slip [26].

Chichili *et al*. [12] and Leclercq *et al*. [13] also found twinning to be the predominant mechanism in the deformation of unalloyed α titanium. However, the tests carried out by them were conducted at much higher loading rates than used in the present study. In addition, they also observed a direct correspondence between twin density and applied stress. Hence, the increase in strength with increasing strain rate (see Table II and Fig. 2) can be explained by the increase in density of twins at higher strain rates.

Interestingly, the deformation behaviour of the titanium alloy over the quasi-static loading range can be correlated from Fig. 4. Metallographic study has shown that during the slow deformation of the titanium alloy, grain boundary sliding is promoted resulting in the increase in microcracks nucleation (see Fig. 7). In other words, plastic work is gradually expended during plastic deformation to initiate grain boundary microcracks by dislocation slip. The dissipation of the plastic energy in the low strain-rate region (10^{-5}–$10^{-4}\ s^{-1}$) is observed in Fig. 4 as a gradual decrease in the strain rate sensitivity of the material.

At the high strain-rate region ($10^{-1}\ s^{-1}$), the strain-rate sensitivity of the material is observed in Fig. 4 to be almost flat for a large part of plastic deformation, but drops sharply at large strain. It is not difficult to imagine that the plastic work is accumulated in the material during fast deformation, suppressing grain boundary sliding or nucleation of microcracks. This is well supported by the fact that the strain-hardening rate of the material was lower at higher loading rates.

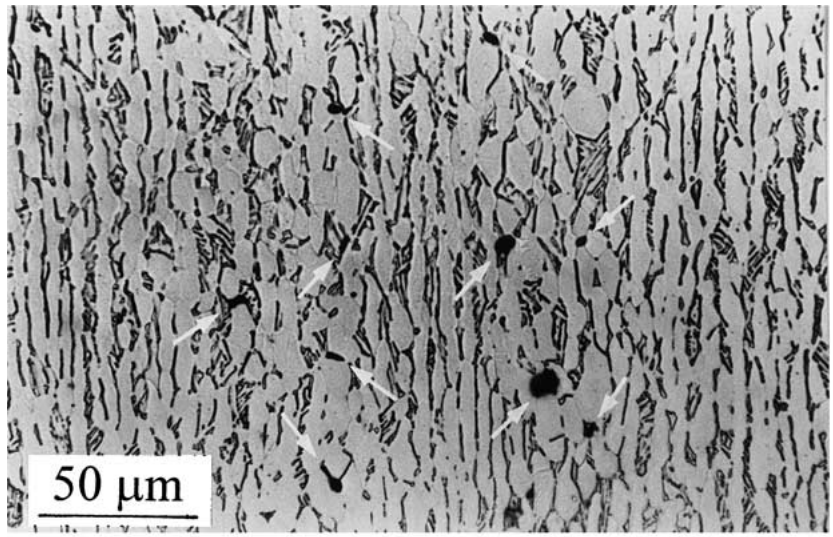

(a)

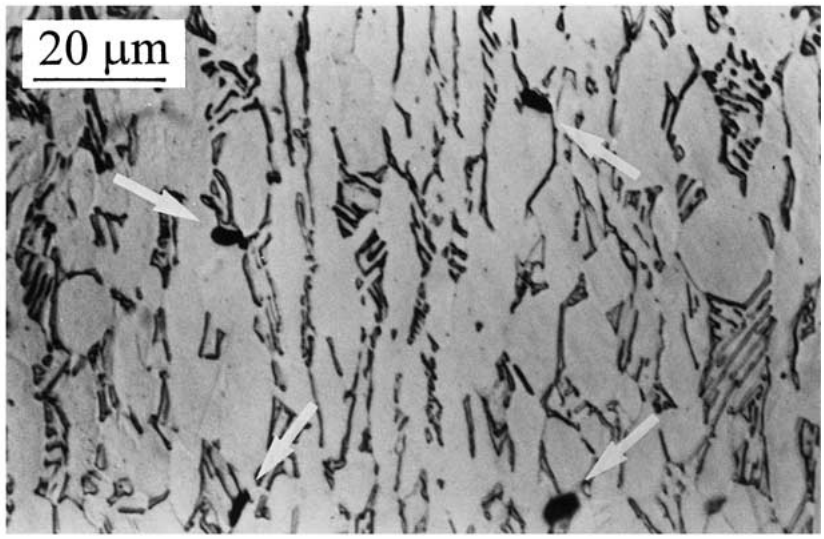

(b)

Figure 7 (a) Microcracks (arrowed) observed in a metallographic sample sectioned from the necked region of a tested tensile specimen along the loading axis. The strain rate employed for the specimen was the lowest at 4.68×10^{-5} s^{-1}. (b) Close up of the grain boundary microcracks. Note that all the microcracks were initiated at grain boundaries oriented roughly at 45 degrees to the loading axis (vertical).

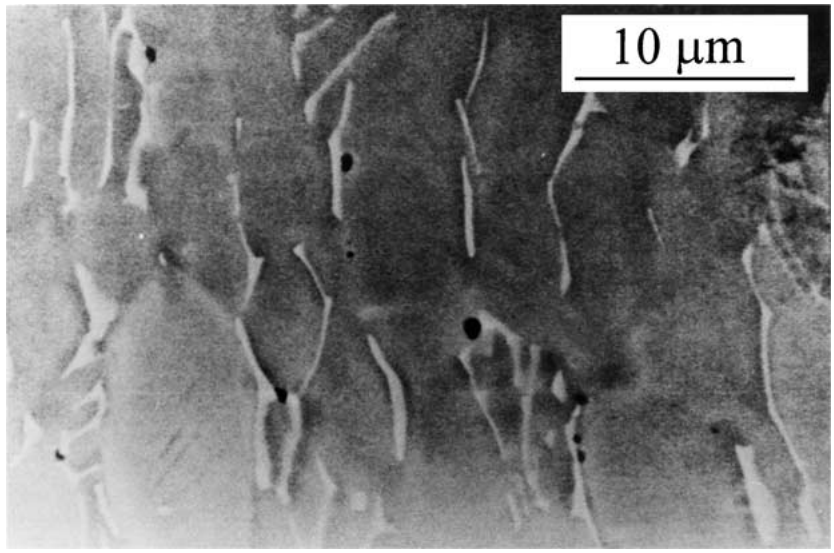

Figure 8 SEM micrograph showing microcracks nucleated at either α grain triple points or α/β interface. It is noted that the β platelets appear white under the SEM.

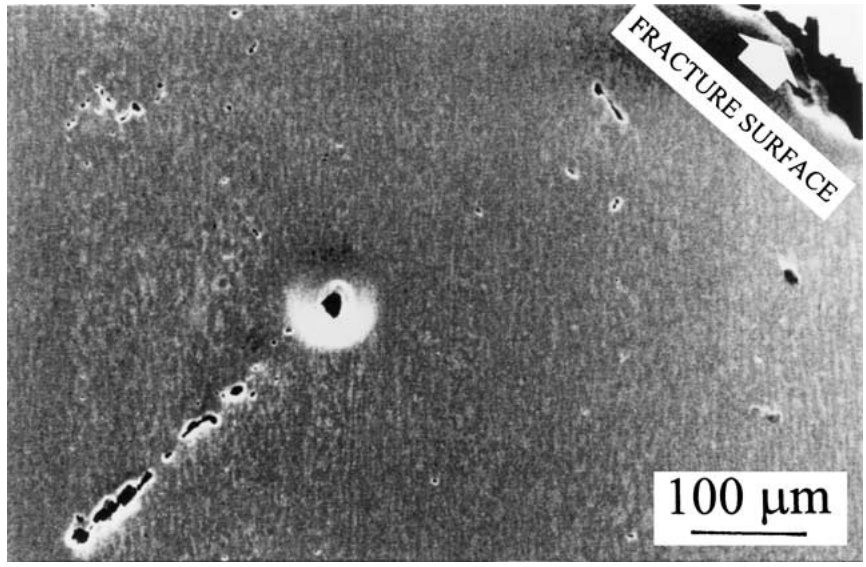

Figure 9 SEM micrograph showing the coalescence of microcracks in highly strained region close to the fracture surface. It can be noted again that both fracture surface and the coalesced cracks are oriented roughly at 45 degrees to the loading direction (vertical).

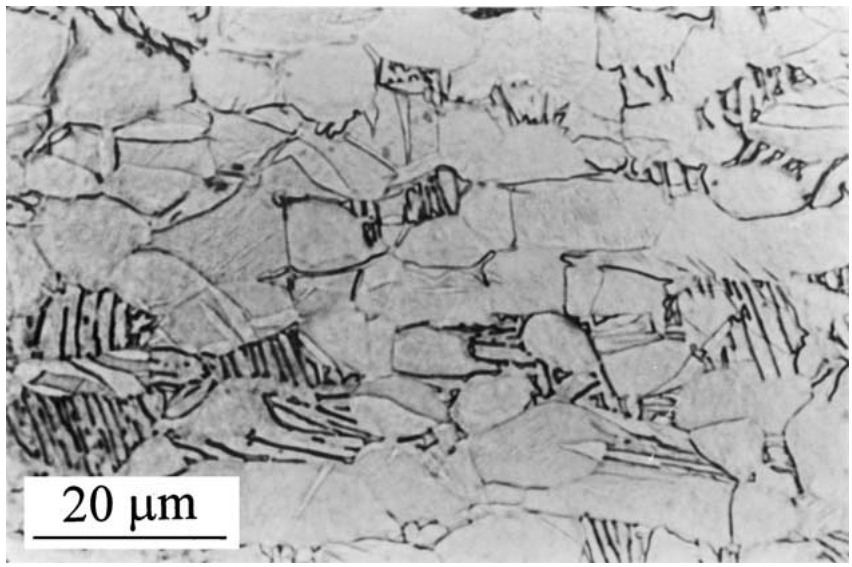

Figure 10 Optical micrograph showing deformation twins in the highly strained neck region sectioned in the axis normal to the loading direction. It is noted that twinning features were observed only in specimens tested at the highest strain rate of $4.68 \times 10^{-1}\,s^{-1}$.

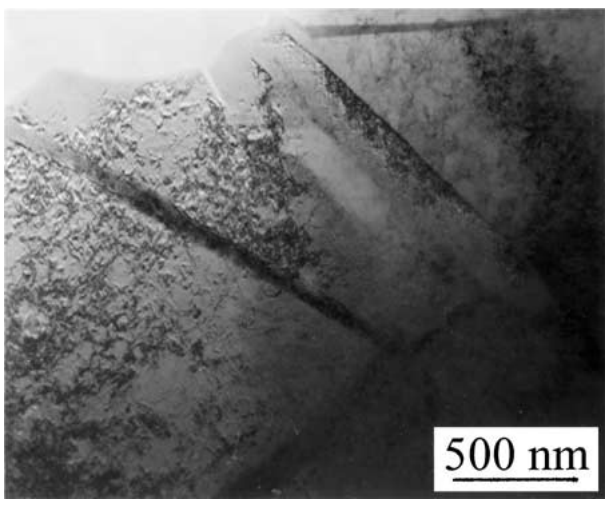

Figure 11 TEM micrograph showing close up of the twinning features in specimens tested at the highest strain rate of $4.68 \times 10^{-1}\,s^{-1}$.

5. Summary and conclusions

The Ti-6A1-4V titanium alloy was observed to have a bimodal $\alpha + \beta$ microstructure. Tensile specimens of the alloy were tested over a large quasi-static loading range (10^{-5}–$10^{-1}\,s^{-1}$) in ambient environment. It was found that strength of the alloy increases but ductility decreases with increasing loading rate. The fracture mode was observed to be predominantly transgrunular, but the fracture was initiated at grain boundaries. Grain boundary sliding through dislocation slip is responsible for the intergranular crack initiation at slow strain rates, but the process is suppressed and twinning occurs when the strain rate is high. The increase in twin density at high strain rates accounts for the increase in strength of the alloy. The strain-rate sensitivity curves plotted for four typical strain-rate regions show good correlation with the physical findings. In the low strain-rate region, strain rate sensitivity decreases gradually during plastic

deformation. In the high strain-rate region, strain-rate sensitivity of the material is largely flat for most part of the plastic deformation.

Acknowledgements

The authors would like to thank Mr. Desmond Tan and Mr. C. M. Tay of Singapore Technologies Automotive Ltd. for the provision of material, Mr. K. C. Soh of Defence Material Organisation (Singapore) for helpful discussion, and Nanyang Technological University for the financial support.

References

1. S. ASHLEY, *Mechanical Engineering* **115** (1993) 60.
2. J. S. MONGOMERY, M. G. H. WELLS, B. ROOPCHAND and J. W. OGILVY, *JOM* **49**(5) (1997) 45.
3. A. M. SHERMAN, C. J. SOMMER and F. H. FROES, *ibid.* **49**(5) (1997) 38.
4. G. SRIDHAR and D. S. SARMA, *Metallurgical & Materials Transactions* **19A** (1988) 3025.
5. Y. KIM, *Acta Metallurgica et Materialia* **40** (1992) 1121.
6. A. A. POPOV, I. Y. PYSHMINTSEV, S. L. DEMAKOV, A. G. ILLARIONOV, T. C. LOWE, A. V. SERGEYEVA and R. Z. VALIEV, *Scripta Materialia* **37** (1997) 1089.
7. C. T. LIU and P. J. MAZIASZ, *Intermetallics* **6** (1998) 653.
8. R. R. BOYER and J. A. HALL, in "Titanium '92: Science and Technology," edited by F. H. Froes and I. L. Caplan (The Minerals, Metals and Materials Society, Warrendale, 1993) p. 77.
9. G. T. TERLINDE, T. W. DUERIG and J. C. WILLIAMS, *Metallurgical Transactions A* **14** (1983) 2101.
10. C. F. CLARKE, D. HARDIE and B. M. IKEDA, *Corrosion Science* **39** (1997) 1545.
11. T. YASHIKI, Y. SUGIZAKI, K. MORI, H. YANO, H. SATOH, Y. ITO, H. ISHIMOTO and Y. TOMOYASU, in "Titanium '95: Science and Technology, edited by P. A. Blenkinsop, W. J. Evans and H. M. Flower (The Institute of Materials, London, 1996) p. 1871.
12. D. R. CHICHILI, K. T. RAMESH and K. J. HEMKER, *Acta Materialia* **46** (1998) 1025.
13. S. LECLERCQ, C. NGUY and P. BENSUSSAN, in "Mechanical Properties of Materials at High Rates of Strain, edited by J. Harding (IOP Publishing Ltd., Great Britain, 1989) p. 299.
14. P. S. FOLLANSBEE and G. T. GRAY, III, *Metallurgical Transactions A* **20** (1989) 863.
15. W. S. LEE and C. F. LIN, *Materials Science and Engineering A* **241** (1998) 48.
16. D. MACDOUGALL and J. HARDING, in "Metallurgical and Materials Applications of Shock-Waves and High-Strain-Rate Phenomena," edited by L. E. Murr, K. P. Staudhammer and M. A. Meyers (Elsevier, New York, 1995) p. 909.
17. M. J. PHILIPPE, in "Titanium '95: Science and Technology," edited by P. A. Blenkinsop, W. J. Evans and H. M. Flowers (The Institute of Materials, London, 1996) p. 956.
18. M. A. MEYERS, in "Dynamic Behavior of Materials" (John Wiley & Sons, Inc., New York, 1994) p. 448.
19. G. E. DIETER, in "Mechanical Metallurgy" (McGraw Hill, New York, 1986) p. 275.
20. W. S. LEE and H. F. LAM, *Journal of Materials Processing Technology* **57** (1996) 233.
21. G. A. LANGE, in "Systematic Analysis of Technical Failures," edited by G. A. Lange (Deutsche Gesellschaft fuer Metallkunde, Germany, 1986) p. 77.
22. T. G. LANGDON, *Acta Metallurgical et Materialia* **42** (1994) 2437.
23. H. G. SUZUKI and D. EYLON, *Materials Science and Engineering A* **243** (1998) 126.
24. K. J. HSIA, D. M. PARKS and A. S. ARGON, *Mechanics of Materials* **11** (1991) 43.
25. J. F. KNOTT, in "Fundamentals of Fracture Mechanics" (Butterworths, London, 1981) p. 211.
26. M. A. MEYERS, in "Dynamic Behavior of Materials" (John Wiley & Sons, Inc., New York, 1994) p. 362.

Received 11 November 1999
and accepted 20 August 2002